

A possible spin Jahn-Teller material: ordered pseudobrookite FeTi_2O_5

Hao-Hang Xu¹, Jian Liu⁴, L.L. Tao¹, Xian-Jie Wang^{1,*}, Sergey V. Streltsov^{2,3*} and Yu Sui^{1,4,*}

¹*School of Physics, Harbin Institute of Technology, Harbin 150001, China*

²*Institute of Metal Physics, S. Kovalevskoy Street 18, Ekaterinburg 620990, Russia*

³*Ural Federal University, Mira Street 19, Ekaterinburg 620002, Russia*

⁴*Laboratory for Space Environment and Physical Sciences, Harbin Institute of Technology, Harbin 150001, China*

Abstract

We investigated the spin-lattice coupling in orthorhombic pseudobrookite FeTi_2O_5 single crystal with highly ordered $\text{Fe}^{2+}/\text{Ti}^{4+}$ occupation, which consists of quasi-1D $S=2$ chains running along a -axis. Both the magnetization and specific heat measurements confirm that the antiferromagnetic phase transition of FeTi_2O_5 occurs at $T_N = 42$ K. The structural distortions were also observed around T_N in the thermal expansion $\Delta L/L(T)$ data. Moreover, the magnetic field was found to strongly affect the thermal expansion both along chains and in the perpendicular direction clearly signaling a substantial magnetoelastic coupling, which was recently proposed to be the origin of a rare spin Jahn-Teller effect, when frustration is lifted via additional lattice distortions. Experimentally observed change in the thermal conductivity slope around T_N is usually associated with the orbital ordering, but DFT+U calculations do not detect modification of the orbital structure across the transition. However, the first-principles calculation results confirm that FeTi_2O_5 is a quasi-1D magnet with a ratio of frustrating inter-chain to intra-chain exchanges $J'/J = 0.03$ and a substantial single-ion anisotropy ($A = 4\text{K}$) of easy-axis type making this material interesting for studying quantum criticality in transverse magnetic fields.

I. INTRODUCTION

The Jahn-Teller (JT) effect is a spontaneous structural distortion that lifts the orbital degeneracy of the d -electron, resulting in the orbital ordering and causing various fascinating phenomena, e.g. it can affect magnetic structure [1], lead to the orbital-selective Mott transition [2] or the reduction of effective dimensionality [3]. In analogy to the JT effect, Yamashita *et al.* proposed the spin JT effect, when the spin degeneracy in geometrical frustration spin systems is released by the structural distortion through the spin-lattice coupling [4]. While this mechanism was initially proposed for ZnV_2O_4 and MgV_2O_4 , it was later also applied to other spinels [5–7].

The orthorhombic pseudobrookite CoTi_2O_5 was recently proposed by Kirschner *et al.* as another candidate for spin JT effect [8]. It was suggested that the triangular geometrical frustration exists in the orthorhombic pseudobrookite CoTi_2O_5 and an unexpected long-range antiferromagnetic ordering of Co^{2+} at $T_N \sim 26$ K is due to an additional structural distortion induced by the spin-lattice coupling through the spin JT effect [8]. Combined the X-ray diffraction measurements on polycrystalline samples with the density functional theory calculations, Lang *et al.* demonstrated that the pseudobrookite FeTi_2O_5 has the same crystal and magnetic structures as CoTi_2O_5 , so the triangular geometrical frustration also exists in FeTi_2O_5 , as shown in Fig.1(a), and a structural distortion is also expected in FeTi_2O_5 [9], but no direct experimental evidence was found. This is not surprising since distortions related to lowering of the crystal structure due to the spin JT effect are expected to be extremely small and are unlikely to be measured by neutron or X-ray diffraction techniques. This remains the situation in multiferroics, where electric polarization is measurable, but corresponding distortions often remain experimentally elusive. In addition, compounds with octahedrally coordinated Fe^{2+} could also exhibit various interesting physical properties due to the orbital ordering of Fe^{2+} . For instance, the orbital ordering of Fe^{2+} accompanied by a structural distortion in perovskite KFeF_3 opens a band gap in the electronic band structure, leading to a metal-insulator transition [10]. Moreover, there is an interplay between charge, spin, and lattice degrees of freedom in famous Fe_3O_4 , which results in formation of trimerons and Verwey transition [11]. Therefore, it is interesting to study coupling between all these degrees of freedom in FeTi_2O_5 as well.

There are two main structural units in the pseudobrookite FeTi_2O_5 : Fe^{2+}O_6 and Ti^{4+}O_6 octahedrons. Like in many other pseudobrookites [12,13], the cations order-disorder also occurs in FeTi_2O_5 ($Cmcm$ space group) due to the existence of the inequivalent $M1\text{O}_6$ and $M2\text{O}_6$ octahedrons, where M represents the $\text{Fe}^{2+}/\text{Ti}^{4+}$ ions. For the highly ordered FeTi_2O_5 , Fe^{2+} ($r = 0.76$ Å) and Ti^{4+} ($r = 0.68$ Å) will occupy the larger $M1\text{O}_6$ octahedron and the smaller $M2\text{O}_6$ octahedron, respectively. However, since the $3d$ shell

of Ti^{4+} ions is completely unoccupied, the unusual magnetic and structural properties of this material are believed to be related to Fe $3d$ electrons [9]. Therefore, there will be no magnetic frustration in FeTi_2O_5 once the vertices of the triangle in Fig.1 (a) are occupied by nonmagnetic Ti^{4+} . Since the frustration is necessary for the spin JT effect, highly ordered $\text{Fe}^{2+}/\text{Ti}^{4+}$ occupancy is needed for investigating the spin JT effect in FeTi_2O_5 . On the other hand, for the completely ordered FeTi_2O_5 , the distance between adjacent Fe^{2+} along the b and c directions is much larger than that along the a -axis ($a = 3.74098 \text{ \AA}$, $b = 9.7609 \text{ \AA}$, $c = 10.0914 \text{ \AA}$) [9], so the 1D $S = 2$ chains of Fe^{2+} are formed along the a -axis. The appearance of the 1D spin chain can result in various fascinating phenomena, e.g. the Bose-Einstein condensation, formation of quantum spin-liquid states, and Haldane phase [14-16], making FeTi_2O_5 attractive for studying also from this perspective.

In this paper, using the floating zone method, the FeTi_2O_5 single crystal with highly ordered $\text{Fe}^{2+}/\text{Ti}^{4+}$ occupation was successfully grown. Through thermal expansion and magnetostriction measurements, we found that the magnetoelastic coupling exists in FeTi_2O_5 .

II. EXPERIMENTAL AND CALCULATION DETAILS

A FeTi_2O_5 single crystal was grown by the optical floating zone technique in an image furnace with two ellipsoidal mirrors (IR Image Furnace G3, Quantum Design Japan). The crystal was grown in the pure Ar atmosphere with a growth rate of 1 mm/h. MgTi_2O_5 single crystal was also prepared under the same condition in order to estimate the lattice specific heat of FeTi_2O_5 . The phase purity was identified by the X-ray diffraction (XRD, Aeris, $\text{CuK}\alpha_1$ radiation) and the X-ray Laue back diffraction was used to confirm the quality of the crystal and determine the crystal principal axes. The magnetic susceptibility and magnetization measurements were performed by using a commercial superconducting quantum interference device magnetometer (MPMS3). The measurement of specific heat $C(T)$ was performed by the physical property measurement system (PPMS, DynaCool-14 T). Both the thermal expansion $\Delta L/L_0(T)$ and the magnetostriction $\Delta L/L_0(H)$ were performed in PPMS by using AH 2550A capacitance dilatometer that was calibrated with 99.999% pure Cu and Al rods. The thermal conductivity $\kappa(T)$ is measured in PPMS with the “one heater, two thermometers” method.

We used density functional theory calculations as realized in the VASP package [17] with generalized gradient approximation (GGA) and the exchange-correlation potential in PBE form [18] to study the electronic and magnetic properties of FeTi_2O_5 . The correlation effects were taken into account by the GGA+U approach [19] with $U-J_H = 4$ eV for Fe and $U-J_H = 2.5$ eV, close to typical values of Hubbard repulsion (U) and intra-atomic exchange used in the literature [20,21]. All calculations were performed for the

9x9x5 mesh of the Brillouin zone, the convergence criterion was set to 10^{-5} eV, while the cut-off energy was chosen to be 500 eV. Following Wigner-Seitz radii were chosen for calculations of atomic charges and magnetic moments: $R_{Fe}=1.302$ Å, $R_{Ti}=1.323$ Å, and $R_O=0.82$ Å.

III. RESULTS AND DISCUSSION

A. X-ray diffraction and magnetic susceptibility

To identify the degree of the ordering of Fe^{2+}/Ti^{4+} in $FeTi_2O_5$, the powder XRD was measured and the Rietveld refinement was performed to identify the degree of the ordering of Fe^{2+}/Ti^{4+} in $FeTi_2O_5$, as shown in Fig.1(b). The refined lattice parameters for room temperature are $a = 3.74014(2)$ Å, $b = 9.76375(6)$ Å, and $c = 10.08496(7)$ Å, as listed in Table I, consistent with the results reported before [9]. From the refinement results, we can also get the information of the Fe^{2+}/Ti^{4+} disorder parameter X in $FeTi_2O_5$, which is defined as the atomic concentration of Ti^{4+} in TM1 sites [22]. For the grown $FeTi_2O_5$ single crystal, X is only 0.12, which is smaller than 0.14 for the well-studied pseudobrookite $MgTi_2O_5$ ceramics with highly ordered Mg^{2+}/Ti^{4+} occupation [22]. So, in our $FeTi_2O_5$ single crystal, most of the Fe^{2+} occupy the $M1$ sites, forming the Fe^{2+} chain along the a -axis.

The temperature dependence of magnetic susceptibilities of $FeTi_2O_5$ single crystal along different axes are displayed in Fig. 2. The rapid decrease at $T_N = 42$ K in the $\chi(T)$ curve along the b -axis of $FeTi_2O_5$ corresponds to the long-range antiferromagnetic ordering of Fe^{2+} , consistent with the previous report [9], while the susceptibilities along the a -axis and the c -axis turn to increase with decreasing temperature below T_N . The anisotropic behavior of $\chi(T)$ curves suggests that the b -axis is the easy axis in $FeTi_2O_5$. When applying different magnetic fields along the b -axis of $FeTi_2O_5$, as shown in Fig. 2(b), T_N decreases with increasing the field and the rapid drop in the magnetic susceptibility tends to disappear. The temperature dependence of magnetic susceptibility of $FeTi_2O_5$ above 90 K was fitted by the Pade approximation following Ref. [23]. The fitting yields nearest neighbor exchange interaction $J_{NN} \sim 22$ K if the Heisenberg model is defined as

$$H_{Heis} = \sum_{i>j} J_{ij} S_i S_j \quad (1)$$

and g -factors along different axes are $g_a \sim 2.24$, $g_b \sim 2.20$, and $g_c \sim 2.30$, which is in accordance with the small difference in the susceptibilities for three different directions at 300 K. As shown in Fig.2 (c), by fitting the $1/\chi$ - T curve of $FeTi_2O_5$ with the Curie-Weiss law from 200 K to 300 K, the effective magnetic moments along the a , b , and c axes were obtained as $5.96 \mu_B$, $5.59 \mu_B$, and $6.35 \mu_B$, respectively, which are much larger

than the spin-only value of $4.90 \mu_B$ for the Fe^{2+} with $S = 2$, indicating that there is an orbital contribution to the magnetic moment in FeTi_2O_5 .

The field dependence of magnetization of FeTi_2O_5 presented in Fig. 2 (d) also confirmed the existence of the orbital contribution. Indeed, $M(H)$ curves along the a - and the c -axis of FeTi_2O_5 deviate from linearity at substantial fields and do not saturate even at about 100 kOe, suggesting a strong magnetic anisotropy due to unquenched orbital moment and substantial spin-orbit coupling. As mentioned above, the 1D chains of Fe^{2+} will be formed along the a -axis in FeTi_2O_5 with highly ordered $\text{Fe}^{2+}/\text{Ti}^{4+}$ occupation. This quasi-one-dimensionality is manifested by the broad peak at around 75 K in the $\chi(T)$ curve, as shown in the inset of Fig. 2(a). Although the Fe^{2+} chains exist in FeTi_2O_5 , the magnetic structure of FeTi_2O_5 is 3D. This is also consistent with the high Neel temperature in FeTi_2O_5 ($T_N \sim 42$ K) which suggests a large interchain exchange interaction in FeTi_2O_5 . However, care should be taken in this respect, since in some low-dimensional materials the ordering temperature is largely suppressed by the logarithm of ratio intra and interchain exchanges [24].

The large interchain exchange interaction in the FeTi_2O_5 having a triangular motif as shown in Fig. 1(a) can result in a geometrical frustration being antiferromagnetic. The frustration index commonly estimated as $|\theta_{CW}|/T_N$ varies from 2.9 to 5.0 for FeTi_2O_5 because the fitted Weiss temperature θ_{CW} differs along different axes. Lang *et al.* proposed that the long-range antiferromagnetic ordering in FeTi_2O_5 appears if the frustration is released by the spin Jahn-Teller effect [9], but no structural distortion has been detected so far.

B. Thermal expansion, specific heat, and thermal conductivity

We measured the temperature dependence of thermal expansion ($\Delta L/L_{80\text{K}}$) of FeTi_2O_5 single crystal along different axes, where the value of $\Delta L/L_{80\text{K}}$ was normalized as $[L(T)-L(80\text{K})]/L(80\text{K})$, as shown in Figs. 3(a) and 3(b). As the temperature decreases, the a -axis of FeTi_2O_5 shows the positive thermal expansion behavior with two anomalies around T_N at 41 K and 43 K, respectively, while the negative thermal expansion appears along the b -axis, and the slope of the $\Delta L/L_{80\text{K}}$ curve along the b -axis also changes around T_N . This anomaly is easier to see from the thermal expansion coefficient $\alpha(T) = d[\Delta L(T)/L_{80\text{K}}]/dT$ plot shown in the insets of Fig. 3 (a) and (b). We also performed the magnetostriction measurement to confirm the existence of the spin-lattice coupling in FeTi_2O_5 . As shown in Figs. 3 (c) and (d), the negative and positive magnetostriction effects appear clearly below T_N along the a - and b -axis, respectively, indicating that there is an obvious spin-lattice coupling in FeTi_2O_5 . This magnetostriction can soften the phonons and induce lattice distortions in FeTi_2O_5 at T_N . A similar effect has been reported

for some transition-metal oxides, e.g., for $\text{Fe}_3(\text{PO}_4)_3$ [25], $\text{Bi}_2\text{Fe}_4\text{O}_9$ [21,26]. With decreasing the temperature, the magnitude of magnetostriction of FeTi_2O_5 increases, as shown in Fig.3(c), indicating the enhancement of spin-lattice coupling at low temperature.

The temperature dependence of specific heat of FeTi_2O_5 single crystal was shown in Fig. 4(a). A peak can be seen at $T_N = 42$ K in the $C(T)$ curve, corresponding to the antiferromagnetic ordering of FeTi_2O_5 [9]. As the temperature decreases, a shoulder-type peak appears in the $C(T)$ curve at 41 K. These two peaks are consistent with two anomalies in thermal expansion along the a -axis. This double-peak behavior in $C(T)$ may correspond to two domains of comparable volume. It is tempting to ascribe this effect to two magnetic domains, characterized by propagation vectors $\mathbf{k}_1 = (\frac{1}{2}, \frac{1}{2}, 0)$ and $\mathbf{k}_2 = (-\frac{1}{2}, \frac{1}{2}, 0)$ [8]. These two phases are degenerate and tiny distortions can lift this degeneracy through the spin JT effect, resulting in the formation of several domains. However, one cannot rule out a simpler scenario, when domains appear due to different degrees of stoichiometry, which comes from the mutual substitution of Fe^{2+} and Ti^{4+} . This slightly non-uniform distribution of Fe^{2+} and Ti^{4+} can cause local strains, stabilizing one or another magnetic phases. Finally, the peak at $T_N = 42$ K can be associated with the long-ranged antiferromagnetic ordering, and the peak at 41 K comes from the structural distortion induced by the magnetostriction phenomenon, which is commonly seen in antiferromagnetic oxides below the Neel temperature, e.g. CoO *etc.* [27].

Magnetic contribution to the specific heat $C_m(T)$ of FeTi_2O_5 can be obtained by subtracting the lattice specific heat $C_p(T)$ from the total specific heat of FeTi_2O_5 . The C_p of the FeTi_2O_5 single crystal was estimated from the C_p of the nonmagnetic MgTi_2O_5 single crystal by using the formula $C_p(T)_{\text{FeTi}_2\text{O}_5} = \sqrt{M_{\text{FeTi}_2\text{O}_5}/M_{\text{MgTi}_2\text{O}_5}} C_p(T)_{\text{MgTi}_2\text{O}_5}$, in which $M_{\text{FeTi}_2\text{O}_5}$ and $M_{\text{MgTi}_2\text{O}_5}$ represent the relative molecular masses of FeTi_2O_5 and MgTi_2O_5 , respectively. The magnetic entropy change of FeTi_2O_5 calculated from $\Delta S = \int_{T_1}^{T_2} \frac{C_m}{T} dT$ is $6.41 \text{ J mol}^{-1} \text{ K}^{-1}$ at T_N , which is about 48% of $R \ln(2 \times 2 + 1) \approx 13.37 \text{ J mol}^{-1} \text{ K}^{-1}$ (R is the gas constant) expected for $S=2$ and close to the value of $R \ln 2 \approx 5.76$. The difference between the calculated and the expected value of ΔS may come from two reasons: (i) the magnetic entropy is released far above T_N by the short-range magnetic ordering in the 1D Fe^{2+} spin chains and (ii) due to the spin JT effect.

As an exclusively sensitive probe for the itinerant excitations [28], the thermal conductivity of FeTi_2O_5 single crystal was also measured to further investigate the source of the structural distortions in FeTi_2O_5 . In Fig. 5, the thermal conductivity of FeTi_2O_5

increases monotonically with decreasing temperature and suddenly enhances around T_N , which is more pronounced in the $1/\kappa(T)$ curve, and a cusp occurs at T_N . When applying the magnetic field of 120 kOe, the κ of FeTi_2O_5 below T_N was apparently suppressed. The change of the slope of $1/\kappa$ is commonly seen in the spinel oxides with orbital degrees of freedom and is explained as the result of the orbital ordering [29,30]. Therefore, one may expect that this change in the $1/\kappa(T)$ curve of FeTi_2O_5 also stems from the orbital ordering of Fe^{2+} , which leads to the anomaly in temperature-dependence of $\Delta L/L_{80\text{K}}$, but this hypothesis must be verified by other methods, e.g., X-ray spectroscopy, while our DFT calculations do not detect any changes in the orbital occupations, see next section. So, this slope change may imply the appearance of spin JT in FeTi_2O_5 . Another possibility for the slope changing in $\kappa(T)$ is that the phonons are transferred more efficiently in the ordered phase. Since FeTi_2O_5 is a quasi-1D antiferromagnet with $S = 2$, a spin gap is expected to open in its magnetic excitation spectrum. Therefore, the increase of κ below T_N may also result from the weakening of the scattering of phonons by magnons. Similar effect has been observed in some quasi-1D antiferromagnets, e.g., NaV_2O_5 [31]. The low-temperature peak in the κ - T curve of FeTi_2O_5 around 30 K is commonly seen in solids, resulting from the phonon-phonon scattering [32].

C. First-principles calculations

To check possible modifications of the orbital structure in FeTi_2O_5 and study exchange interaction, we performed GGA and GGA+U calculations. It has to be mentioned that Fe resides in 4c positions in the $Cmcm$ space group [9], which corresponds to the C_{2v} point group. The degeneracy of $3d$ -orbitals is completely lifted in this case. Indeed, results of the Wannier function projection of the non-magnetic GGA Hamiltonian using Wannier90 code [33] for the experimental crystal structure measured for room temperature [9] presented in Fig. 6a confirm general symmetry arguments. Thus, there is no orbital degeneracy to be lifted. The lowest in energy is the xz orbital (in the global coordinate system), which is shown in Fig. 6b. In the high-spin d^6 configuration of Fe^{2+} a single electron with spin-minority must occupy this orbital, and the next in energy orbital is split by 210 meV. Such a large crystal-field splitting agrees with strong distortions of FeO_6 octahedra and disfavors any redistribution of electrons, which is needed for any non-trivial orbital ordering below T_N . Weak distortions due to the spin JT are not expected to strongly affect electronic level structure.

The direct GGA+U calculations confirm that correlation effects do not change the situation and indeed a single electron with spin-minority occupies the xz orbital, making this orbital doubly occupied and inactive in the exchange interaction along the chain. Moreover, we also performed optimization of the crystal structure and calculations taking

into account experimental modifications of lattice parameters according to our thermal expansion measurements (expand along the a -axis and shrink in the b -direction). None of them show changes in the orbital structure.

Fig. 7 shows the density of state plots in the case of GGA+U calculation with spins in the chain ordered antiferromagnetically. One can see that the bottom of the conduction band is formed by completely empty Ti $3d$ states, while the top of the valence band is by Fe $3d$ spin-minority states (narrow bands just below the Fermi level have xz character; corresponding orbital is shown in Fig. 6b). The band gap is ~ 1.7 eV.

Finally, we calculated the exchange interaction parameter for the Heisenberg model (1) using method of 4 configurations [34]. The intra-chain exchange was found to be $J=17.7$ K. This agrees with the fitting of magnetic susceptibility by the Pade approximation of the 1D Heisenberg model as explained above. The diagonal inter-chain exchange (for simplicity we do not differentiate between such exchanges in the ab and ac planes) was calculated to be $J'=0.6$ K.

In addition, GGA+U+SOC (SOC stands for the spin-orbit coupling) calculations reveal that spins are directed along the b -axis with orbital momentum $\sim 0.1\mu_B$. This fully agrees with our magnetization measurements (see Sec. IIIa). The single-ion anisotropy modeled by $H_{SIA} = \sum_i A (S_i^z)^2$ was found to be $A=4$ K from the total energy GGA+U+SOC calculations of 4 configurations: when at one of the spins is directed along b , $-b$, a , or $-a$, while all other spins are along the c axis.

Thus, we see that FeTi_2O_5 exhibits the Ising-like behavior and can be an example of a quasi 1D Ising antiferromagnet with spin $S = 2$. Indeed, ratio of intra- to inter-chain exchanges $J/J' \sim 30$ and $A/J' \sim 7$. This model has highly unusual properties in the presence of the transverse magnetic field. There can be a quantum critical behavior (as the field increases) together with the exotic E_8 excitations. This is now one of the hot subjects in the physics of low-dimensional magnetic systems and material realizations of these phenomena e.g. in 1D ferromagnetic CoNb_2O_6 [35–37] or antiferromagnetic $\text{BaCo}_2\text{V}_2\text{O}_8$ [38–40] are under active studying. However, interest in the Ising model in the transverse field is not restricted by materials with $S=1/2$, since the field induces tunneling processes between states in a double-well potential characterized by different spin projections and these are not necessarily only the states with $S_z=1/2$ [41].

IV. CONCLUSION

The pseudobrookite FeTi_2O_5 single crystal with highly ordered $\text{Fe}^{2+}/\text{Ti}^{4+}$ occupation was grown under the pure Ar atmosphere. Magnetostriction measurements clearly demonstrate the appearance of the magnetoelastic coupling, which is consistent with the previously proposed spin Jahn-Teller scenario of leaving degeneracy in this highly

frustrated system due to coupling with crystal lattice and stabilizing a long-range magnetic order [9]. While tiny distortions associated with the spin Jahn-Teller effect are unluckily to be measured by diffraction techniques, our experiments reveal the existence of magnetoelastic coupling in FeTi_2O_5 and *ab initio* calculations rule out another mechanism of symmetry lowering due to orbital degrees of freedom. In addition, density function theory calculations unravel a substantial easy-axis anisotropy putting this material to the class of quasi 1D Ising model, which agrees with the field dependence of magnetization. Exotic properties of Ising systems in the transverse magnetic fields together with a strong magnetoelastic coupling make FeTi_2O_5 a unique object interesting for further detailed investigation.

ACKNOWLEDGMENTS

We thank Valentin Irkhin, Alexander Vasiliev, Dylan Behr, and Roger Johnston for fruitful discussions and the Synergetic Extreme Condition User Facility (SECUF) for physical properties measurements. This work was supported by National Key R&D Program of China No. 2023YFA1406100, the National Natural Science Foundation of China (Grant No. 52372003) and the Funds from Beijing National Laboratory for Condensed Matter Physics. Work of S.V.S. was supported by “Quantum” program (№ 122021000038-7).

REFERENCES

- [1] J. B. Goodenough, *Theory of the Role of Covalence in the Perovskite-Type Manganites $[\text{La}, \text{M}(\text{II})]\text{MnO}_3$* , Phys. Rev. **100**, 564 (1955).
- [2] M. Neupane, P. Richard, Z.-H. Pan, Y.-M. Xu, R. Jin, D. Mandrus, X. Dai, Z. Fang, Z. Wang, and H. Ding, *Observation of a Novel Orbital Selective Mott Transition in $\text{Ca}_{1.8}\text{Sr}_{0.2}\text{RuO}_4$* , Phys. Rev. Lett. **103**, 097001 (2009).
- [3] D. I. Khomskii and S. V. Streltsov, *Orbital Effects in Solids: Basics, Recent Progress, and Opportunities*, Chem. Rev. **121**, 2992 (2021).
- [4] Y. Yamashita and K. Ueda, *Spin-Driven Jahn-Teller Distortion in a Pyrochlore System*, Phys. Rev. Lett. **85**, 4960 (2000).
- [5] S. KoNDo, C. Urano, Y. Kurihara, M. Nohara, and H. Takagi, *From the Geometrically Frustrated Antiferromagnets ZnV_2O_4 and ZnCr_2O_4 to the Heavymass Fermi Liquid LiV_2O_4* , J. Phys. Soc. Japan **69**, 139 (2000).
- [6] Y. Kino and B. Lüthi, *Magnetic and Elastic Properties of Zinc-Chromite*, Solid State Commun. **9**, 805 (1971).
- [7] V. Tsurkan, H.-A. Nidda, J. Deisenhofer, P. Lunkenheimer, and A. Loidl, *On the Complexity of Spinel: Magnetic, Electronic, and Polar Ground States*, Phys.

- Rep. **926**, (2021).
- [8] F. K. K. Kirschner, R. D. Johnson, F. Lang, D. D. Khalyavin, P. Manuel, T. Lancaster, D. Prabhakaran, and S. J. Blundell, *Spin Jahn-Teller Antiferromagnetism in CoTi₂O₅*, Phys. Rev. B **99**, 064403 (2019).
 - [9] F. Lang, L. Jowitt, D. Prabhakaran, R. D. Johnson, and S. J. Blundell, *FeTi₂O₅: A Spin Jahn-Teller Transition Enhanced by Cation Substitution*, Phys. Rev. B **100**, 94401 (2019).
 - [10] J. Varignon, M. Bibes, and A. Zunger, *Origins versus Fingerprints of the Jahn-Teller Effect in d-Electron ABX₃ Perovskites*, Phys. Rev. Res. **1**, 033131 (2019).
 - [11] M. S. Senn, J.P. Wright, and J.P. Attfield, *Charge order and three-site distortions in the Verwey structure of magnetite*. Nature, **48**, 173 (2012).
 - [12] Y. Suzuki and Y. Shinoda, *Magnesium Dtitanate (MgTi₂O₅) with Pseudobrookite Structure: A Review*, Sci. Technol. Adv. Mater. **12**, 034301 (2011).
 - [13] Y. Ohya, Y. Kawauchi, and T. Ban, *Cation Distribution of Pseudobrookite-Type Titanates and Their Phase Stability*, J. Ceram. Soc. Japan **125**, 695 (2017).
 - [14] V. Zapf, M. Jaime, and C. D. Batista, *Bose-Einstein Condensation in Quantum Magnets*, Rev. Mod. Phys. **86**, 563 (2014).
 - [15] L. Clark and A. H. Abdeldaim, *Quantum Spin Liquids from a Materials Perspective*, Annu. Rev. Mater. Res. **51**, 495 (2021).
 - [16] O.V. Maksimova, S.V. Streltsov, A.N. Vasiliev, *Long range ordered, dimerized, large D and Haldane phases in spin 1 chain compounds*, Critical reviews in solid state and materials sciences **46**, 371 (2021).
 - [17] G. Kresse and J. Furthmüller, *Efficient Iterative Schemes for Ab Initio Total-Energy Calculations Using a Plane-Wave Basis Set*, Phys. Rev. B **54**, 11169 (1996).
 - [18] J. P. Perdew, K. Burke, and M. Ernzerhof, *Generalized Gradient Approximation Made Simple*, Phys. Rev. Lett. **77**, 3865 (1996).
 - [19] S. L. Dudarev, G. A. Botton, S. Y. Savrasov, C. J. Humphreys, and A. P. Sutton, *Electron-Energy-Loss Spectra and the Structural Stability of Nickel Oxide: An LSDA+U Study*, Phys. Rev. B **57**, 1505 (1998).
 - [20] S. V Streltsov, O. A. Popova, and D. I. Khomskii, *Comment on "Sodium Pyroxene NaTiSi₂O₆: Possible Haldane Spin-1 Chain System,"* Phys. Rev. Lett. **96**, 249701 (2006).
 - [21] Z. V Pchelkina and S. V Streltsov, *Ab Initio Investigation of the Exchange Interactions in Bi₂Fe₄O₉: The Cairo Pentagonal Lattice Compound*, Phys. Rev. B **88**, 054424 (2013).
 - [22] M. He, B. Winkler, J. D. Bauer, L. Bayarjargal, J. Ruiz-Fuertes, I. Alencar, W. Morgenroth, K. Refson, and V. Milman, *Lattice Dynamics and Mg/Ti Order in Orthorhombic Pseudobrookite-Type MgTi₂O₅*, J. Alloys Compd. **699**, 16 (2017).
 - [23] J. M. Law, H. Benner, and R. K. Kremer, *Padé Approximations for the Magnetic*

- Susceptibilities of Heisenberg Antiferromagnetic Spin Chains for Various Spin Values*, J. Phys. Condens. Matter **25**, 065601 (2013).
- [24] A. A. Katanin, A. A. Katanin, and V. Y. Irkhin, *Magnetic Order and Spin Fluctuations in Low-Dimensional Insulating Systems*, Physics-Uspekhi **50**, 613 (2007).
- [25] A. Pal et al., *Spin-Induced Strongly Correlated Magnetodielectricity, Magnetostriction Effect, and Spin-Phonon Coupling in Helical Magnet Fe₃(PO₄)₃*, Phys. Rev. B **106**, 094404 (2022).
- [26] I. K. Jeong and N. Hur, *Local Structural Distortion Induced by Antiferromagnetic Ordering in Bi₂Fe₄O₉ Studied Using Neutron Total Scattering Analysis*, J. Korean Phys. Soc. **69**, 75 (2016).
- [27] S. Greenwald, *The Antiferromagnetic Structure Deformations in CoO and MnTe*, Acta Crystallogr. **6**, 396 (1953).
- [28] M. Yamashita et al., *Thermal-Transport Studies of Kagomé Antiferromagnets*, J. Phys. Condens. Matter **32**, 074001 (2020).
- [29] Y. Ishitsuka, T. Ishikawa, R. Koborinai, T. Omura, and T. Katsufuji, *Comparative Studies of the Thermal Conductivity of Spinel Oxides with Orbital Degrees of Freedom*, Phys. Rev. B - Condens. Matter Mater. Phys. **90**, 224411 (2014).
- [30] T. Omura, T. Ishikawa, Y. Ishitsuka, and T. Katsufuji, *Orbital Fluctuations in Spinel Mn(VI-XAl_x)₂O₄ Studied by Thermal Conductivity Measurements*, Phys. Rev. B **86**, 054436 (2012).
- [31] M. Markina, A. Vasiliev, J. Mueller, M. Lang, K. Kordonis, T. Lorenz, M. Isobe, and Y. Ueda, *Thermal Properties of NaV₂O₅*, J. Magn. Magn. Mater. **258–259**, 398 (2003).
- [32] B. Ramachandran, K. K. Wu, Y. K. Kuo, and M. S. Ramachandra Rao, *Phonon Thermal Transport and Phonon–Magnon Coupling in Polycrystalline BiFeO₃ Systems*, J. Phys. D: Appl. Phys. **48**, 115301 (2015).
- [33] G. Pizzi et al., *Wannier90 as a Community Code: New Features and Applications*, J. Phys. Condens. Matter **32**, 165902 (2020).
- [34] H. Xiang, E. Kan, S.-H. Wei, M.-H. Whangbo, and X. Gong, *Predicting the spin-lattice order of frustrated systems from first principles*. Physical Review B, **84**, 224429 (2011).
- [35] R. Coldea, D. A. Tennant, E. M. Wheeler, E. Wawrzynska, D. Prabhakaran, M. Telling, K. Habicht, P. Smeibidl, and K. Kiefer, *Quantum Criticality in an Ising Chain: Experimental Evidence for Emergent E₈ Symmetry*, Science (80-.). **327**, 177 (2010).
- [36] M. Fava, R. Coldea, and S. A. Parameswaran, *Glide Symmetry Breaking and Ising Criticality in the Quasi-1D Magnet CoNb₂O₆*, Proc. Natl. Acad. Sci. **117**, 25219 (2020).
- [37] C. M. Morris et al., *Duality and Domain Wall Dynamics in a Twisted Kitaev*

- Chain*, Nat. Phys. **17**, 832 (2021).
- [38] Q. Faure et al., *Topological Quantum Phase Transition in the Ising-like Antiferromagnetic Spin Chain BaCo₂V₂O₈*, Nat. Phys. **14**, 716 (2018).
- [39] S. K. Niesen, G. Kolland, M. Seher, O. Breunig, M. Valldor, M. Braden, B. Grenier, and T. Lorenz, *Magnetic Phase Diagrams, Domain Switching, and Quantum Phase Transition of the Quasi-One-Dimensional Ising-like Antiferromagnet BaCo₂V₂O₈*, Phys. Rev. B **87**, 224413 (2013).
- [40] X. Wang, K. Puzniak, K. Schmalzl, C. Balz, M. Matsuda, A. Okutani, M. Hagiwara, J. Ma, J. Wu, and B. Lake, *Spin Dynamics of the E₈ Particles*, (2023).
- [41] S. Suzuki, J. Inoue, and B. K. Chakrabarti, *Quantum Ising Phases and Transitions in Transverse Ising Models*, Vol. 862 (Springer Berlin Heidelberg, Berlin, Heidelberg, 2013).

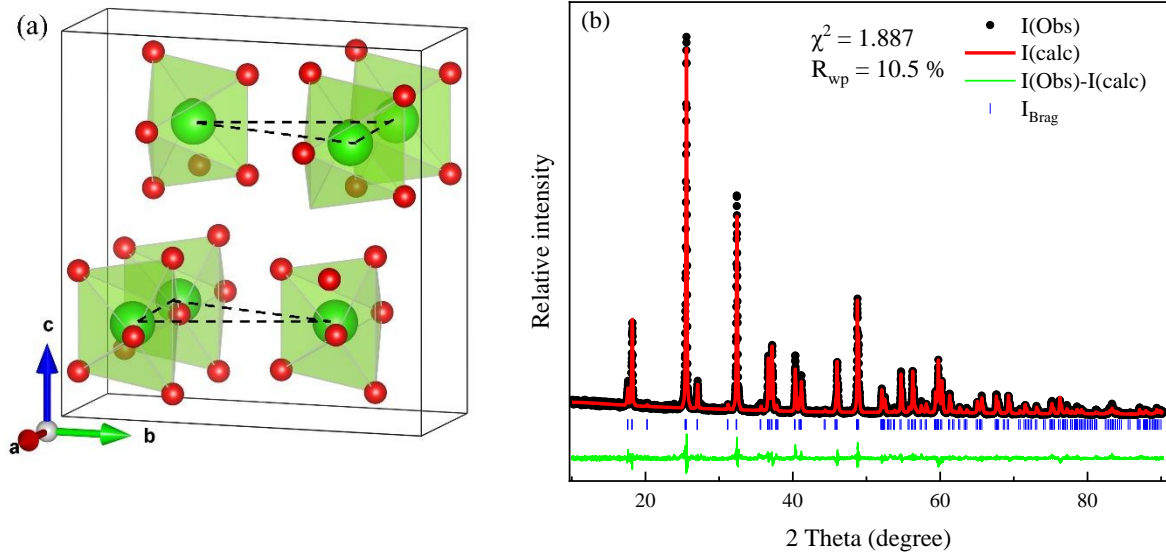


FIG.1 (a) The schematic diagram of the geometrical frustration in FeTi_2O_5 , in which only Fe^{2+} (the green ball) and the corner-shared O^{2-} (the red ball) were shown. Fe chains run along a -axis. The dashed line shows the triangular geometric frustration in FeTi_2O_5 .
 (b) The Rietveld refinement results of FeTi_2O_5 .

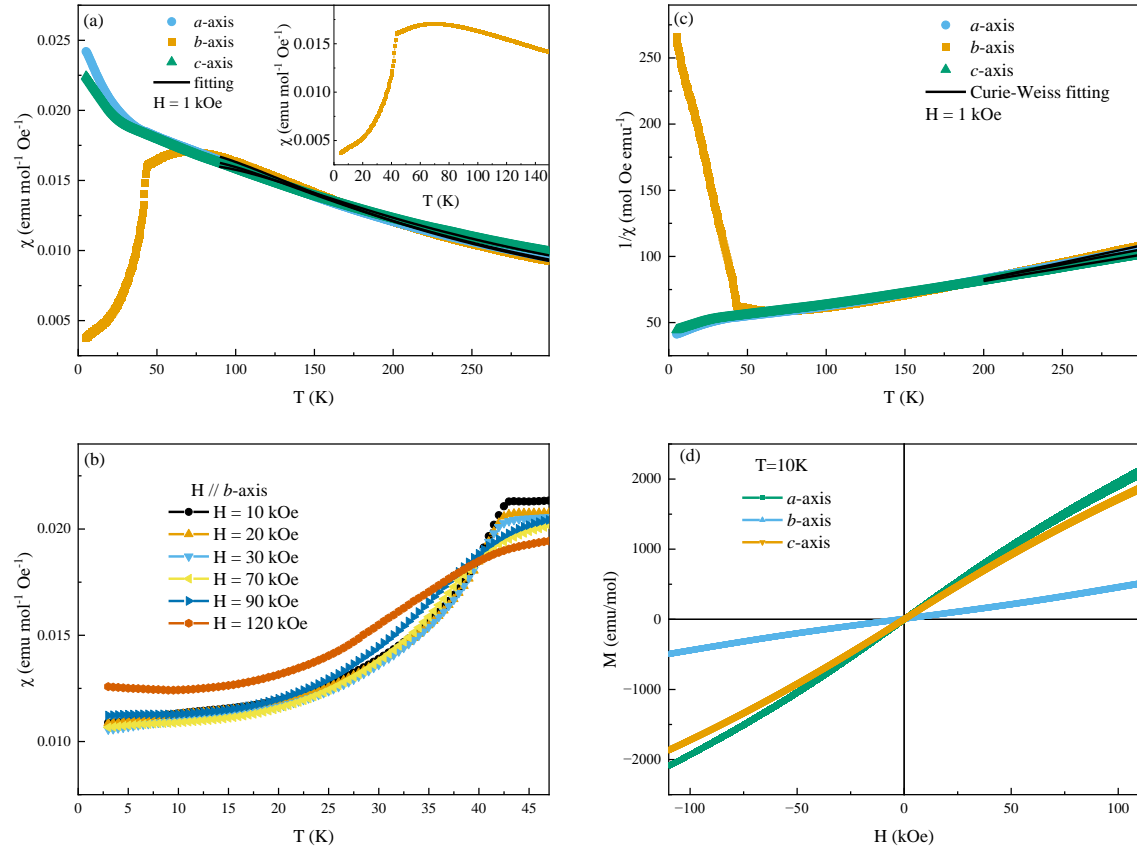


FIG.2 The magnetic measurements of FeTi₂O₅ single crystal along different axes. (a) χ - T . The inset presents the broad peak along the b -axis in enlarged form. (b) Low-temperature susceptibilities at different fields along the b -axis. (c) $1/\chi$ - T . (d) $M(H)$ curves.

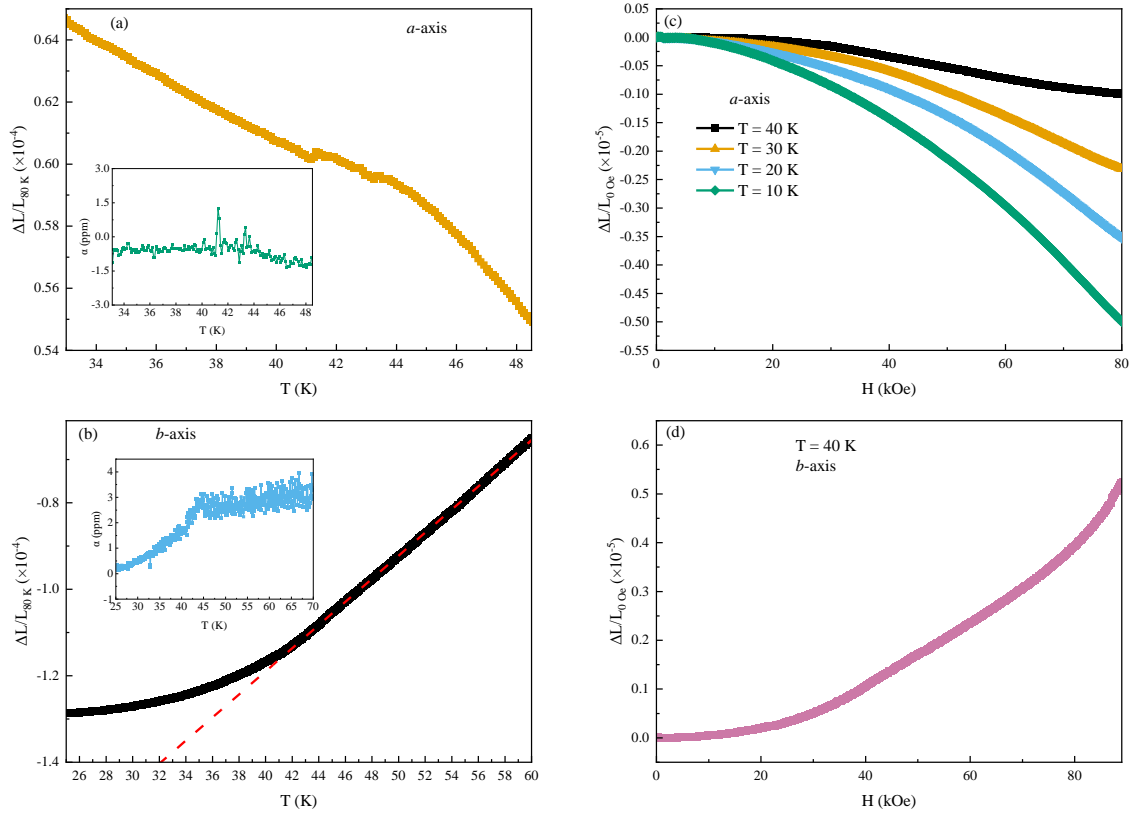


FIG.3 (a) and (b) The thermal expansion of FeTi₂O₅ single crystal along the a -axis and b -axis. The insets show the thermal expansion coefficient α of FeTi₂O₅. (c) The magnetostriction of FeTi₂O₅ single crystal along the a -axis at different temperatures. (d) The magnetostriction of FeTi₂O₅ single crystal along the b -axis below T_N .

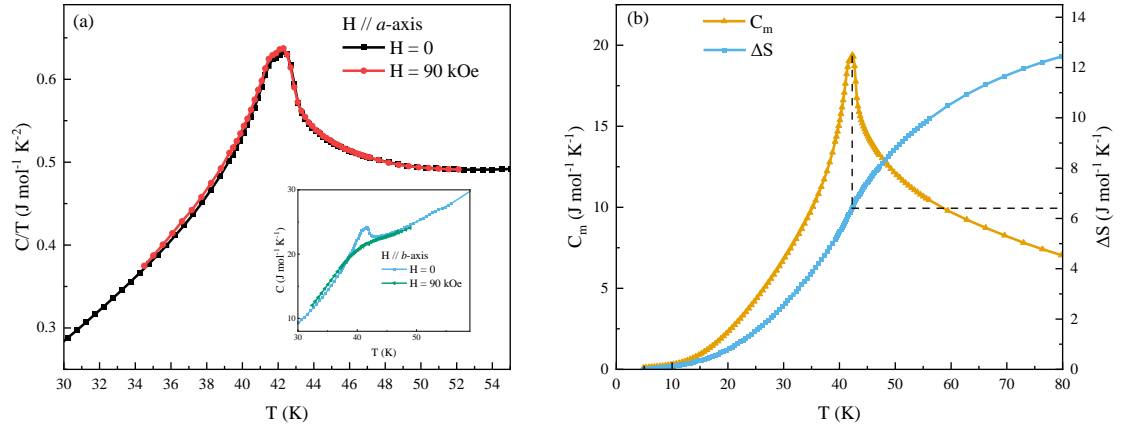


FIG. 4 (a) The specific heat of FeTi₂O₅ under different magnetic fields. (b) The magnetic specific heat and change of magnetic entropy of FeTi₂O₅.

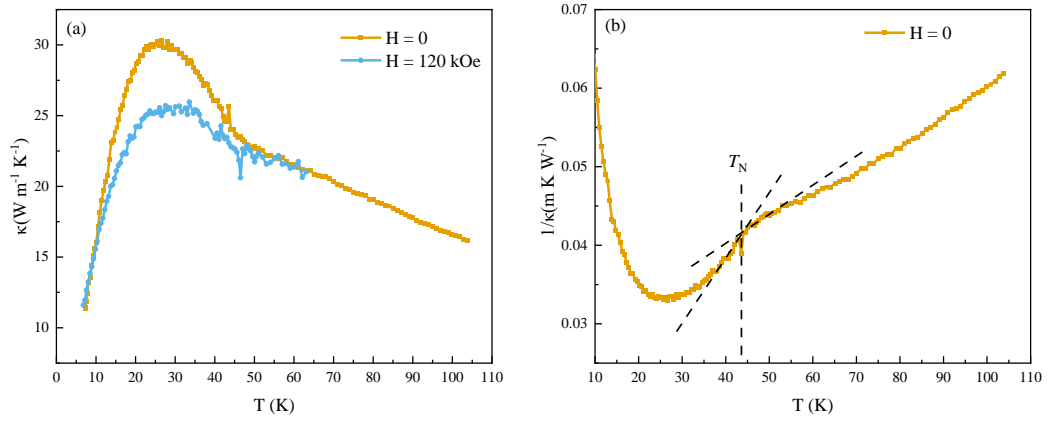


FIG. 5 The thermal conductivity of FeTi₂O₅ single crystal along the *a*-axis under different magnetic fields. (a) κ - T , (b) $1/\kappa$ - T . The dashed line in the $1/\kappa$ - T at zero field is used to show the change in the slope.

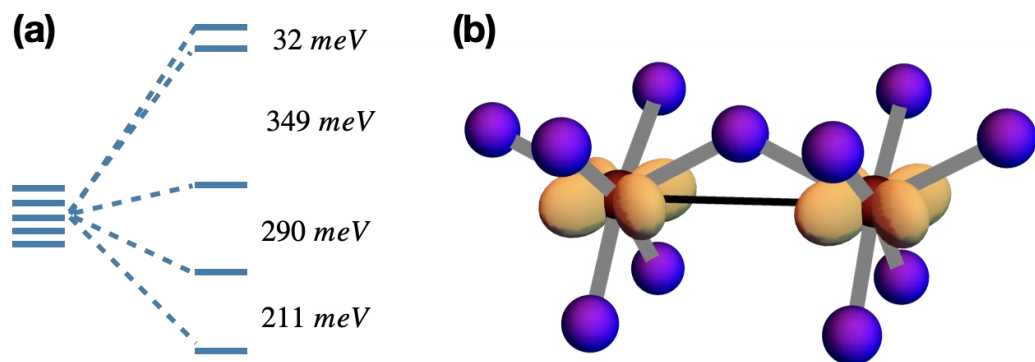


Fig. 6 (a) Crystal-field splitting of the Fe 3d shell as obtained by the Wannier function projection of non-magnetic GGA calculations. (b) the lowest in energy xz orbital (in the global coordinate system) in GGA non-magnetic calculations; Fe ions are shown by red, while O is by violet balls.

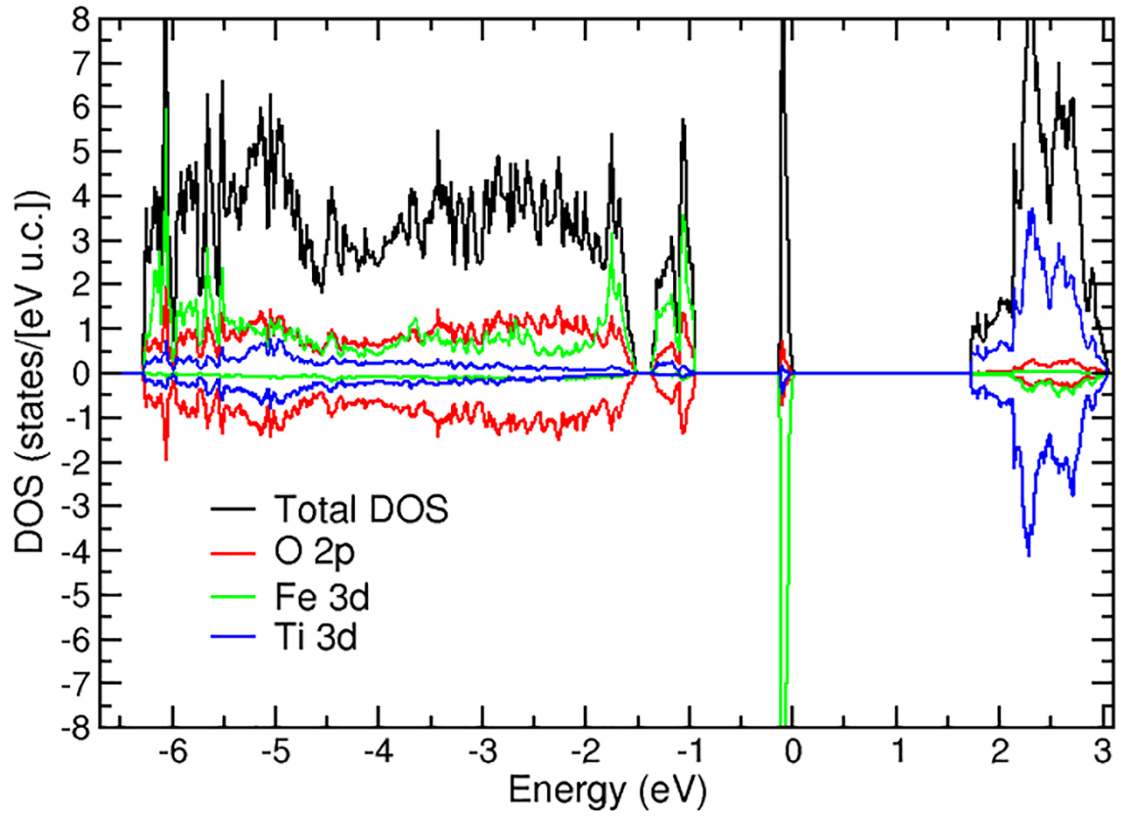


Fig. 7 Total and partial densities of states (DOS) as obtained in GGA+U calculations for the magnetic configuration, where spins in the same chain are AFM ordered. For O $2p$, Fe $3d$, and Ti $3d$ two spin projections are shown by (positive DOS for spin majority, negative for spin minority). The Fermi level is set to zero.

TABLE I. Refined crystal structure parameters of FeTi₂O₅

Cell parameters					
Space group: <i>Cmcm</i>					
<i>a, b, c</i> (Å) 3.74014(2) 9.76375(6) 10.08496(7)					
Atomic fractional coordinates					
Atom	Site	<i>a</i>	<i>b</i>	<i>c</i>	Occ.
Fe1	4 <i>c</i>	0	0.1916	0.2500	0.8885
Ti1	4 <i>c</i>	0	0.1916	0.2500	0.1115
Fe2	8 <i>f</i>	0	0.1343	0.5666	0.0558
Ti2	8 <i>f</i>	0	0.1343	0.5666	0.9442
O1	4 <i>c</i>	0	0.7810	0.2500	1.0000
O2	8 <i>f</i>	0	0.0450	0.1130	1.0000
O3	8 <i>f</i>	0	0.3150	0.0610	1.0000